2015

CONSTRAINED DIVERGENCE-CONFORMING BASIS FUNCTIONS FOR METHOD OF MOMENTS DISCRETIZATIONS IN ELECTROMAGNETICS

Robert Pfeiffer
University of Kentucky, robpfeiffer@gmail.com

STUDENT AGREEMENT:

I represent that my thesis or dissertation and abstract are my original work. Proper attribution has been given to all outside sources. I understand that I am solely responsible for obtaining any needed copyright permissions. I have obtained needed written permission statement(s) from the owner(s) of each third-party copyrighted matter to be included in my work, allowing electronic distribution (if such use is not permitted by the fair use doctrine) which will be submitted to UKnowledge as Additional File.

I hereby grant to The University of Kentucky and its agents the irrevocable, non-exclusive, and royalty-free license to archive and make accessible my work in whole or in part in all forms of media, now or hereafter known. I agree that the document mentioned above may be made available immediately for worldwide access unless an embargo applies.

I retain all other ownership rights to the copyright of my work. I also retain the right to use in future works (such as articles or books) all or part of my work. I understand that I am free to register the copyright to my work.

REVIEW, APPROVAL AND ACCEPTANCE

The document mentioned above has been reviewed and accepted by the student's advisor, on behalf of the advisory committee, and by the Director of Graduate Studies (DGS), on behalf of the program; we verify that this is the final, approved version of the student's thesis including all changes required by the advisory committee. The undersigned agree to abide by the statements above.

Robert Pfeiffer, Student

Dr. John Young, Major Professor

Dr. Caicheng Lu, Director of Graduate Studies

CONSTRAINED DIVERGENCE-CONFORMING BASIS FUNCTIONS FOR METHOD OF MOMENTS DISCRETIZATIONS IN ELECTROMAGNETICS

THESIS

A thesis submitted in partial fulfillment of the
requirements for the degree of Master of Science
in Electrical Engineering in the College of Engineering
at the University of Kentucky

By

Robert Pfeiffer

Lexington, Kentucky

Director: Dr. John Young

Lexington, Kentucky

2015

ABSTRACT OF THESIS

CONSTRAINED DIVERGENCE-CONFORMING BASIS FUNCTIONS FOR METHOD OF MOMENTS DISCRETIZATIONS IN ELECTROMAGNETICS

Higher-order basis functions are widely used to model currents and fields in numerical simulations of electromagnetics problems because of the greater accuracy and computational efficiency they can provide. Different problem formulations, such as method of moments (MoM) and the finite element method (FEM) require different constraints on basis functions for optimal performance, such as normal or tangential continuity between cells. In this thesis, a method of automatically generating bases that satisfy the desired basis constraints is applied to a MoM formulation for scattering problems using surface integral equations. Numerical results demonstrate the accuracy of this approach, and show good system matrix conditioning when compared to other higher-order bases.

KEYWORDS: Basis Functions, Method of Moments, Electromagnetics, Constrained Basis Functions, Computational Electromagnetics, System Conditioning

Robert A. Pfeiffer

August 20, 2015

CONSTRAINED DIVERGENCE-CONFORMING BASIS FUNCTIONS FOR METHOD OF MOMENTS DISCRETIZATIONS IN ELECTROMAGNETICS

By

Robert Pfeiffer

Dr. John Young
Director of Thesis

Dr. Caicheng Lu
Director of Graduate Studies

August 20, 2015

ACKNOWLEDGEMENTS

JMJ

I must first express my sincere thanks to my advisor Dr. John C. Young. His guidance and assistance throughout this project, and his constant readiness to address my many tedious questions and difficulties, have made the writing of this thesis and the research behind it an instructive and enjoyable experience.

Moreover, I would like to thank Dr. Robert Adams and Dr. Caicheng Lu for serving on my defense committee; the class instruction they have both given me has also helped me greatly in my research.

I must also express my gratitude to Dr. Jovan Jevtić and Dr. Cory Prust for the careful instruction and thoughtful advice they gave me during my studies at the Milwaukee School of Engineering.

I am indebted to all of my teachers at Thomas Aquinas College for the logical and philosophical foundation they helped me to build, but especially to Dr. Michael Letteney, Dr. Michael Augros, and Dr. Glen Coughlin. Their thorough instruction in the principles and methods of Mathematics and Natural Science has proven invaluable during my graduate studies.

Finally, I would like to thank my family for their loving care and moral support during my college career, especially my parents. Their heroic dedication in raising and homeschooling a large family stands among God's greatest blessings in my life, and inspires me in all things to strive for excellence.

TABLE OF CONTENTS

LIST OF TABLES

LIST OF FIGURES

1. INTRODUCTION

The use of higher-order basis functions in method-of-moments (MoM) discretizations allows for more accurate solutions to integral equations in electromagnetics without increasing mesh refinement [1]. Unfortunately, integral equation solutions to Maxwell's equations result in dense system matrices due to convolution with the Green's function. For problems with large numbers of unknowns, dense system matrices rapidly become impractical and various fast solvers have been proposed to decrease both solution time and memory requirements. Performance of these fast solvers, however, is critically dependent on the system conditioning, which is related to things such as integral equation formulation, mesh density, basis function order and type, etc. In this paper we employ "constrained" bases similar to those in [2] in MoM formulations of electromagnetic scattering problems. These basis functions, tailored to each cell or pair of cells in the mesh, are constructed from scaled Legendre polynomials for orthogonality and result in a significant reduction in system matrix condition number.

As the complexity and electrical size of scattering structures grow, high-order basis functions are used to retain accuracy without resorting to mesh refinement. Some relatively simple functions such as the power-based functions of [3] or the interpolatory Glisson-Wilton-Peterson (GWP) functions of [4] serve this purpose. While these bases are well suited to direct matrix solvers, the high condition numbers of the resulting system matrices do not lend themselves as readily to solution by iterative or fast solvers [5].

For larger MoM problems, fast methods such as iterative or sparse direct solvers are, in general, the only feasible option. Fast methods are sensitive to the system matrix conditioning, so the selection of basis functions that do not degrade the matrix condition number can significantly increase efficiency in solving large problems. In this thesis, we define a "well-conditioned" basis set to be a basis function set that does not degrade the system condition number significantly with increasing basis order. As pointed out in [1], the conditioning can be improved by choosing basis and test functions that are more nearly orthogonal to each other, which requires, in the case of Galerkin testing, that the basis functions be as mutually orthogonal as possible. While the requirement of normal continuity of basis functions across cell boundaries and/or the use of curvilinear meshing make perfect orthogonality difficult to achieve [1], close approximations to orthogonality have dramatically [1, 5] improved the system conditioning over those using power-based and other non-orthogonal basis sets. Many of these methods employ the already mutually orthogonal Legendre polynomials as bases or use the Gramm-Schmidt procedure to orthogonalize higher-order functions with respect to each other [6]. Clever combinations or modifications of Legendre polynomials to achieve near orthogonality are reported in [1]. These methods give system matrix conditioning several orders of magnitude lower than the interpolatory bases of [4], and the condition number grows much more slowly with increasing basis order [1, 5].

Sumic et al [7] derive a set of "maximally orthogonalized" higher-order basis functions from Legendre polynomials which exhibit a significant improvement in conditioning. These functions do not have rigidly determined forms but are constructed by solving systems of equations involving inner products of Legendre polynomials.

In this paper, the constrained basis approach used previously in a locally corrected Nyström code in [2, 8] is applied to a MoM formulation. This approach, originating from ideas concerning Helmholtz decompositions in [9, 10], is a more general way of constructing basis functions, starting from only a set of constraints and an underlying function set. Like the bases of [7], the final forms of the proposed bases are not given explicitly but are determined by the solution of a system of equations for each cell or edge in the mesh. The system is relatively simple, however, and does not involve integration to find the inner product between many pairs of functions. The singular value decomposition of this system yields vectors of coefficients that correctly weight a predetermined set of functions so that the weighted sum is a basis satisfying the desired constraints. For typical basis orders, this procedure has little computational cost and not only gives a far more flexible and general method for constructing bases than those previously proposed but also automatically brings about a significant improvement in matrix conditioning. Results in this paper show condition numbers significantly lower than those of [1] and comparable to those of [5].

In this thesis, the method-of-moments (MoM) context in which the constrained bases are employed and the general theory of the constrained basis approach with its particular application to quadrilateral surface MoM problems are described. Numerical results for error convergence are given to validate the accuracy of the proposed method, and system condition numbers for various scattering geometries are given for comparison with conditioning in other published results.

2. THEORY

2.1. The Method of Moments

Scattering problems involving perfect electrical conductors (PEC) can be solved using the electric field integral equation (EFIE) [11]

$$\hat{\mathbf{n}} \times \mathbf{E}^{\text{inc}}(\mathbf{r}) - j\eta k \hat{\mathbf{n}} \times \iint_S G(\mathbf{r},\mathbf{r}')\mathbf{J}(\mathbf{r}')ds' - j\frac{\eta}{k}\hat{\mathbf{n}} \times \nabla \iint_S G(\mathbf{r},\mathbf{r}')\nabla' \cdot \mathbf{J}(\mathbf{r}')ds' = \mathbf{0}, \tag{1}$$

where the equation is enforced for $\mathbf{r} \in S$. If the scattering surface is closed, the magnetic field integral equation (MFIE) [12]

$$\hat{\mathbf{n}} \times \mathbf{H}^{\text{inc}}(\mathbf{r}) + \lim_{\mathbf{r} \downarrow S} \hat{\mathbf{n}} \times \nabla \times \oiint_S \mathbf{J}(\mathbf{r}')G(\mathbf{r},\mathbf{r}')dS' = \mathbf{J}(\mathbf{r}), \qquad \mathbf{r} \in S \tag{2}$$

may also be used. The notation $\lim_{\mathbf{r} \downarrow S}$ in equation (2) indicates that the integral is enforced in the limit as $\mathbf{r} \to S$ from a point exterior to *S*. Here, *G* is the free-space Green's function

$$G(\mathbf{r},\mathbf{r}') = \frac{e^{-jk|\mathbf{r}-\mathbf{r}'|}}{4\pi|\mathbf{r}-\mathbf{r}'|}, \tag{3}$$

S is the surface of the scatterer, $\mathbf{E}^{\text{inc}}$ and $\mathbf{H}^{\text{inc}}$ are the incident fields, $\mathbf{J}$ is the surface current over *S*, and $\hat{\mathbf{n}}$ is a unit normal to S that is oriented outward when S is closed. Also, $k = \omega\sqrt{\mu\varepsilon}$ is the wave number and $\eta = \sqrt{\mu/\varepsilon}$ the wave impedance where μ and ϵ are the permeability and permittivity of the medium, respectively. Both the EFIE and MFIE give spurious solutions for a closed surface at the discrete frequencies associated with the internal resonances of the surface [13]. One remedy for this breakdown is to use a combined field integral equation (CFIE) that is a linear combination of the EFIE and MFIE [13].

A more concise expression is possible with the use of the operators $\mathcal{T}$ and $\mathcal{K}$ where

$$\mathcal{T}(\mathbf{F},\mathbf{r}) = -j\eta k \iint_S G(\mathbf{r},\mathbf{r}')\mathbf{F}(\mathbf{r}')ds' - j\frac{\eta}{k}\nabla\iint_S G(\mathbf{r},\mathbf{r}')\nabla'\cdot\mathbf{F}(\mathbf{r}')ds' \tag{4}$$

$$\mathcal{K}(\mathbf{F},\mathbf{r}) = \nabla\times\oiint_S \mathbf{F}(\mathbf{r}')G(\mathbf{r},\mathbf{r}')dS' = \oiint_S \mathbf{F}(\mathbf{r}')\times\nabla' G(\mathbf{r},\mathbf{r}')dS' \tag{5}$$

Physically, $\mathcal{T}(\mathbf{J},\mathbf{r})$ and $\mathcal{K}(\mathbf{J},\mathbf{r})$ represent the electric and magnetic fields, respectively, at a field point **r** radiated by an electric current density **J**. One can now rewrite (1) and (2) as

$$\hat{\mathbf{n}}\times\mathbf{E}^{\text{inc}}(\mathbf{r}) + \hat{\mathbf{n}}\times\mathcal{T}(\mathbf{J},\mathbf{r}) = \mathbf{0}, \qquad \mathbf{r}\in S \tag{6}$$

and

$$\hat{\mathbf{n}}\times\mathbf{H}^{\text{inc}}(\mathbf{r}) + \lim_{\mathbf{r}\downarrow S}\hat{\mathbf{n}}\times\mathcal{K}(\mathbf{J},\mathbf{r}) = \mathbf{J}(\mathbf{r}), \qquad \mathbf{r}\in S\ . \tag{7}$$

The limiting operation in the MFIE can be removed by noting that

$$\lim_{\mathbf{r}\downarrow S}\hat{\mathbf{n}}\times\mathcal{K}(\mathbf{J},\mathbf{r}) = \frac{1}{2}\mathbf{J}(\mathbf{r}) + \hat{\mathbf{n}}\times\text{P.V.}\left(\mathcal{K}(\mathbf{J},\mathbf{r})\right), \qquad \mathbf{r}\in S \tag{8}$$

where P.V. indicates a principal value integral. Use of (8) in (7) gives

$$\hat{\mathbf{n}}\times\mathbf{H}^{\text{inc}}(\mathbf{r}) + \hat{\mathbf{n}}\times\mathcal{K}(\mathbf{J},\mathbf{r}) = \frac{1}{2}\mathbf{J}(\mathbf{r}), \qquad \mathbf{r}\in S\ , \tag{9}$$

where the P.V. notation is suppressed and should be apparent from context. If **J(r)** is approximated in terms of *N* known basis functions $\mathbf{B}_n(\mathbf{r})$ with unknown coefficients β_n as

$$\mathbf{J}(\mathbf{r}) \approx \sum_{n=1}^{N} \beta_n \mathbf{B}_n(\mathbf{r}), \tag{10}$$

then the EFIE can be expressed as

$$\hat{\mathbf{n}} \times \mathbf{E}^{\text{inc}}(\mathbf{r}) = -\sum_{n=1}^{N} \beta_n \hat{\mathbf{n}} \times \mathcal{T}(\mathbf{B}_n, \mathbf{r}), \quad \mathbf{r} \in S \ . \tag{11}$$

Note that each $\mathbf{B}_n$ should lie on *S* and be tangential to S since it represents a physical, induced current. A set of testing functions $\mathbf{T}_m$ for $m = 1, \ldots, N$ that also lie tangential to *S* can now be used to discretize the EFIE into the system of equations

$$\begin{aligned} \left\langle \hat{\mathbf{n}} \times \mathbf{T}_m, \hat{\mathbf{n}} \times \mathbf{E}^{\text{inc}} \right\rangle &= -\left\langle \hat{\mathbf{n}} \times \mathbf{T}_m, \sum_{n=1}^{N} \beta_n \hat{\mathbf{n}} \times \mathcal{T}(\mathbf{B}_n) \right\rangle \\ &= -\sum_{n=1}^{N} \beta_n \left\langle \hat{\mathbf{n}} \times \mathbf{T}_m, \hat{\mathbf{n}} \times \mathcal{T}(\mathbf{B}_n) \right\rangle, \quad m = 1, \ldots, N \end{aligned} \ , \tag{12}$$

where the scalar product $\langle \mathbf{F}_1(\mathbf{r}), \mathbf{F}_2(\mathbf{r}) \rangle$ is defined by

$$\langle \mathbf{F}_1, \mathbf{F}_2 \rangle = \iint_S \mathbf{F}_1(\mathbf{r}) \cdot \mathbf{F}_2(\mathbf{r}) dS \ . \tag{13}$$

Since

$$\hat{\mathbf{n}} \times \mathbf{F}_1 \cdot \hat{\mathbf{n}} \times \mathbf{F}_2 = \mathbf{F}_1 \cdot \mathbf{F}_2 \tag{14}$$

if at least one of $\mathbf{F}_1$ or $\mathbf{F}_2$ is perpendicular to $\hat{\mathbf{n}}$, i.e., tangential to *S*, (12) reduces to

$$\left\langle \mathbf{T}_m, \mathbf{E}^{\text{inc}} \right\rangle = -\sum_{n=1}^{N} \beta_n \left\langle \mathbf{T}_m, \mathcal{T}(\mathbf{B}_n) \right\rangle \ . \tag{15}$$

This gives the matrix equation

$$\bar{E} = [Z]\bar{\beta} \tag{16}$$

where

$$Z_{mn} = -\left\langle \mathbf{T}_m, \mathcal{T}(\mathbf{B}_n) \right\rangle \tag{17}$$

and

$$E_m = \left\langle \mathbf{T}_m, \mathbf{E}^{\text{inc}} \right\rangle \ . \tag{18}$$

The MFIE can be similarly discretized from

$$\left\langle \mathbf{T}_m, \hat{\mathbf{n}} \times \mathbf{H}^{\text{inc}} \right\rangle = \sum_{n=1}^{N} \beta_n \left\{ \frac{1}{2} \left\langle \mathbf{T}_m, \mathbf{B}_n \right\rangle - \left\langle \mathbf{T}_m, \hat{\mathbf{n}} \times \mathcal{K}(\mathbf{B}_n) \right\rangle \right\}, \quad m = 1, \ldots, N \tag{19}$$

to give the matrix equation

$$\bar{H} = [Y]\bar{\beta} \tag{20}$$

where

$$Y_{mn} = \frac{1}{2} \left\langle \mathbf{T}_m, \mathbf{B}_n \right\rangle - \left\langle \mathbf{T}_m, \hat{\mathbf{n}} \times \mathcal{K}(\mathbf{B}_n) \right\rangle \tag{21}$$

and

$$H_m = \left\langle \mathbf{T}_m, \hat{\mathbf{n}} \times \mathbf{H}^{\text{inc}} \right\rangle \ . \tag{22}$$

The CFIE is formed by the linear combination of (16) and (20) to give

$$\alpha \bar{E} + \eta(1-\alpha)\bar{H} = \left(\alpha[Z] + \eta(1-\alpha)[Y]\right)\bar{\beta} \tag{23}$$

where $0 < \alpha < 1$.

2.2. Higher-Order Basis Functions

In formulating the method of moments problem, the surface is meshed with, possibly curvilinear, quadrilateral or triangular cells. The basis functions used to model the current are each non-zero only on a cell or pair of cells. When a basis function

represents current that does not flow from one cell to its neighbor, and so has support only on a single mesh element, it is called a *face* basis. A basis function that is nonzero on two adjacent cells, however, is referred to as an *edge* basis and represents current flowing across the shared edge.

As elements in a mesh discretization become finer, the current becomes almost constant over each cell, except near sharp edges. Thus, even simple bases that give only a low-order approximation of the current can yield a high degree of accuracy with sufficient discretization. The computational expense of the solution, however, grows extremely rapidly as the mesh is refined, and so higher-order basis functions are often preferred for modeling current. These bases not only are more economical, but also result in exponential convergence with mesh refinement for smooth structures.

2.3. Constrained Bases

The choice of the basis set $\mathbf{B}_n$ and the test set $\mathbf{T}_n$ has a significant influence on the solver performance. High-order bases can greatly improve accuracy without mesh refinement but can also result in poorly conditioned system matrix, which, as mentioned above, can drastically affect the computational efficiency of fast solvers.

The divergence operator in the last term of (1) indicates the importance of normal continuity of current between mesh elements to prevent the presence of boundary charges. Similar conditions are necessary in other methods—FEM formulations, for example, require tangential continuity of bases across cell boundaries to maintain finite curl.

Typically, basis functions are chosen that analytically satisfy the appropriate continuity constraints on all cells throughout the problem. Choosing bases that improve properties such as system conditioning can, however, be difficult. A more general and flexible approach is to take a set of functions $\{\mathbf{P}_q(\mathbf{r})\}$, capable of spanning the desired basis space, with an appropriate set of constraints, and to determine specifically for each basis the linear combination of these functions that satisfies the given constraints. This general approach is used to build the constrained bases proposed here.

In practice, the constrained bases are constructed by picking an appropriate number Q of such functions $P_q(\mathbf{r})$ and enforcing their linear combination to take some value at an appropriate set of points $\mathbf{r}_p$ in the basis domain. Typically, the points lie on the cell boundaries ℓ of the cell or cells on which the basis is defined. For example, for divergence conforming bases one may enforce

$$\sum_{q=1}^{Q} \alpha_q \hat{\mathbf{e}}^1(\mathbf{r}_p) \cdot \mathbf{P}_q^1(\mathbf{r}_p) = 0, \quad \mathbf{r}_p \in \ell_b \tag{24}$$

at mesh edges ℓ_b on the boundary of an object or

$$\sum_{q=1}^{Q} \alpha_q^1 \hat{\mathbf{e}}^1(\mathbf{r}_p) \cdot \mathbf{P}_q^1(\mathbf{r}_p) = -\sum_{q=1}^{Q} \alpha_q^2 \hat{\mathbf{e}}^2(\mathbf{r}_p) \cdot \mathbf{P}_q^2(\mathbf{r}_p), \quad \mathbf{r}_p \in \ell_c \tag{25}$$

along shared (common) mesh edges ℓ_c . Here, $\hat{\mathbf{e}}^n(\mathbf{r}_p)$ is the unit normal to the edge at $\mathbf{r}_p$, pointing out of and tangential to the n^{th} cell. For bases on adjacent cells that must be constrained relative to each other (e.g., must be continuous across the shared edge), (25) is used, where the superscripts distinguish cells. For N constraints and Q functions, matrix equations of the form

$$\left[C\right]\bar{\beta}^n = [C^{f,n}]\bar{\beta}^n = \bar{0} \tag{26}$$

for face bases and

$$\left[C\right]\begin{bmatrix}\bar{\beta}^m \\ \bar{\beta}^n\end{bmatrix} = \begin{bmatrix}\left[C^{f,n}\right] & [0] \\ \left[C^{e,m}\right] & \left[C^{e,n}\right] \\ [0] & \left[C^{f,m}\right]\end{bmatrix}\begin{bmatrix}\bar{\beta}^m \\ \bar{\beta}^n\end{bmatrix} = \bar{0} \tag{27}$$

for edge bases can be constructed. $\bar{0}$ denotes a zero vector. All matrix elements are of the form $\hat{\mathbf{e}}^n\left(\mathbf{r}_p\right)\cdot\mathbf{P}_q^n\left(\mathbf{r}_p\right)$.

The constraints for each face or edge are thus expressed in a $N\times Q$ constraint matrix $[C]$ with nullity $N-Q$ [2], and so the null space of $[C]$ will contain the coefficients for $N-Q$ linearly independent basis functions that satisfy the chosen constraints. These can be extracted from the matrix $[V]$ of right singular vectors found by taking the singular value decomposition (SVD) of $[C]$ as

$$[C] = [U][\Sigma][V]^H . \tag{28}$$

The $N-Q$ column vectors $[V_0]$ of $[V]$ associated with zero singular values in $[\Sigma]$ are a basis for the null space of $[C]$, and so the columns of $[V_0]$ are valid coefficient vectors $\bar{\beta}$ satisfying (26). Since the dimensions of $[C]$ are small for typical basis orders, the SVD is inexpensive to compute. The matrix $[V]$ is unitary [14], and so the column vectors of $[V_0]$ are linearly independent. Thus, if the functions $\{P_q(\mathbf{r})\}$ are an orthonormal set under a suitable inner product, then their linear combinations weighted by the elements in the vectors in $[V_0]$ are linearly independent basis functions. As

discussed below, components of the edge bases may be dependent on components in the face bases, creating redundancies, though these redundancies can be easily removed with simple matrix algebra.

This summarizes the essence of the constrained basis approach. The more particular task of implementing this method in a MoM formulation with quadrilateral mesh cells is laid out in detail in the following section.

2.4. Constrained Bases for Method of Moments Formulations

In this paper, the proposed constrained-basis method is used to generate divergence-conforming bases on quadrilateral cells in a surface mesh, though in principle the method might be extended to curl-conforming bases as well as other surface or volume mesh elements.

On a quadrilateral surface mesh element parameterized by the coordinates (u^1, u^2) (see Figure 1) the surface current density $\mathbf{J}$ can be decomposed into components parallel to a particular cell's unitary vectors $\mathbf{a}_i = \dfrac{\partial \mathbf{r}}{\partial u^i}$ [15] :

$$\mathbf{J} = \mathbf{J}_1 + \mathbf{J}_2 = J_1 \mathbf{a}_1 + J_2 \mathbf{a}_2 \ . \tag{29}$$

Each component can be expressed as a weighted sum of basis functions $\mathbf{B}_q^i$ as

$$\mathbf{J}_i \approx \sum_{q=1}^{Q} \beta_q^i \mathbf{B}_q^i(\mathbf{r}) \ . \tag{30}$$

where Q is the number of bases used to represent $\mathbf{J}_i$ on a particular cell or pair of cells. We assume in this work that $\mathbf{J}_1$ and $\mathbf{J}_2$ are represented by the same number of bases

although this is not necessary in general. The basis functions $\mathbf{B}_q^i$ can be expressed in terms of the cell's parametric coordinates as

$$\mathbf{B}_q^i(\mathbf{r}) = B_q^i(u^1, u^2)\mathbf{a}_i \ . \tag{31}$$

In EFIE formulations, the divergence operator in (1) reduces the order of $B_q^i(u^i, u^{i+1})$ in the u^i direction by one. Since the divergence of the current is proportional to the charge density, for the charge representation to be complete to order p, the current bases must be of orders $(p+1)$ and p in the u^i and u^{i+1} directions, respectively. This charge-complete representation is desirable to avoid spurious solutions [16].

2.4.1. Face Bases

Independent parametric coordinates and edge numbering for a single quadrilateral cell are defined in Figure 1, with $u^i \in [0,1]$. In what follows, all index arithmetic is modulo 4. Also, $u^0 = 1 - u^2$ and $u^3 = 1 - u^1$. The vector $\hat{\mathbf{e}}_i^n$ is of unit length, and is tangential to the n^{th} cell, normal to the i^{th} edge; $\hat{\mathbf{e}}_i^n$ can be calculated by normalizing the reciprocal unitary vector $\mathbf{a}^i$ as defined in [15]. The current on the n^{th} cell is expressed in terms of the unitary vectors $\mathbf{a}_i$ as

$$\mathbf{J}^n = \mathbf{J}_1^n + \mathbf{J}_2^n = J_1^n \mathbf{a}_1 + J_2^n \mathbf{a}_2 \ . \tag{32}$$

The normal continuity constraint demands that the component of current normal to a cell boundary be continuous across the boundary. For components of the current that do not flow across the edges of the cell, this means that the component normal to each

edge must be zero at that edge. These components, confined as they are to a single cell or face, are referred to as *face* bases. The face basis constraints can be expressed by

$$\mathbf{J}^n(\mathbf{r})\cdot\hat{\mathbf{e}}_k^n(\mathbf{r}) = J_1^n\mathbf{a}_1^n(\mathbf{r})\cdot\hat{\mathbf{e}}_k^n(\mathbf{r}) + J_2^n\mathbf{a}_2^n(\mathbf{r})\cdot\hat{\mathbf{e}}_k^n(\mathbf{r}) = 0, \quad \mathbf{r}\in\ell_k^n, \quad k=0,1,2,3. \tag{33}$$

By definition, the unitary vector $\mathbf{a}_{i+1}$ is tangential to the ℓ_i and ℓ_{i+2} edges for $u^i = 0,1$ [4], and so normal continuity of $\mathbf{J}_{i+1}^n$ is guaranteed across these edges irrespective of J_{i+1}^n. Hence, J_i^n need be constrained only on edges ℓ_i and ℓ_{i+2} such that

$$J_i^n\mathbf{a}_i^n(\mathbf{r})\cdot\hat{\mathbf{e}}_k^n(\mathbf{r}) = 0, \quad \mathbf{r}\in\ell_k^n, \quad k=i,i+2 \tag{34}$$

for $i=1$ and $i=2$ independently. $J_i^n(\mathbf{r})$ is now approximated as a linear combination of Q simpler functions $P_q^{i,n}(\mathbf{r})$:

$$J_i^n(\mathbf{r}) = \sum_{q=1}^{Q}\beta_q^{i,n}P_q^{i,n}(\mathbf{r}) \ . \tag{35}$$

The unknown coefficients $\beta_q^{i,n}$ can be determined by enforcing (34) at N_p points along each edge. If J_i^n is polynomial complete to order p in u^{i+1}, then $N_p = p+1$ points are required to ensure that (35) is identically zero over the boundary. The exact location of the points depends on the function space $\{P_q\}$. The face constraints become

$$[\mathbf{a}_i^n(\mathbf{r}_p)\cdot\hat{\mathbf{e}}_k^n(\mathbf{r}_p)]\sum_{q=1}^{Q}\beta_q^{i,n}P_q^{i,n}(\mathbf{r}_p) = 0 \tag{36}$$

for $\mathbf{r}_p\in\ell_k^n$, $p=1,2...N_p$, and $k=i,i+2$. The constraints in (36) for the n^{th} mesh cell can be expressed by the matrix equation

$$\begin{bmatrix} [C^{i,n}] \\ [C^{i+2,n}] \end{bmatrix} \bar{\beta} = \left[C^{face} \right] \bar{\beta} = \bar{0} \ , \tag{37}$$

where

$$C_{pq}^{k,n} = [\mathbf{a}_i(\mathbf{r}_p) \cdot \hat{\mathbf{e}}_k^n(\mathbf{r}_p)] P_q^{i,n}(\mathbf{r}_p), \quad \mathbf{r}_p \in \ell_k^n, \quad k = i, i+2 \ . \tag{38}$$

Equations (35)-(37) apply to both independent current directions in the cell, that is, to both $i = 1$ and $i = 2$.

It is worth noting that only for $p \geq 1$ do face bases exist, since for $p = 0$, $\left[C^{face} \right]$ in (37) is a 2×2 full rank matrix with no null space.

2.4.2. Edge Bases

Currents that flow across shared cell boundaries, called *edge* bases, also obey the constraint in (36) at the edges opposite the shared edge, but on the shared edge the component normal to the edge is not identically zero. Parametric coordinate and edge notation for adjacent cells are illustrated in Figure 2. If the edges ℓ_i^m and ℓ_k^n of the m^{th} and n^{th} cells, respectively, coincide, the continuity constraint on an edge basis that flows across this common edge ℓ_c can be expressed as

$$\mathbf{J}^m(\mathbf{r}) \cdot \hat{\mathbf{e}}_i^m(\mathbf{r}) + \mathbf{J}^n(\mathbf{r}) \cdot \hat{\mathbf{e}}_k^n(\mathbf{r}) = 0, \quad \mathbf{r} \in \ell_c \tag{39}$$

where $\mathbf{J}^p$ signifies the current on the p^{th} cell and $\hat{\mathbf{e}}_q^p$ signifies the outward unit normal to the q^{th} edge on the p^{th} cell. As above, this reduces to

$$J_i^m(\mathbf{r})[\mathbf{a}_i^m(\mathbf{r}) \cdot \hat{\mathbf{e}}_i^m(\mathbf{r})] + J_k^n(\mathbf{r})[\mathbf{a}_k^n(\mathbf{r}) \cdot \hat{\mathbf{e}}_k^n(\mathbf{r})] = 0, \quad \mathbf{r} \in \ell_c \ . \tag{40}$$

When J_i^p is expressed as in (35), the constraints simplify to

$$[\mathbf{a}_i^m \cdot \hat{\mathbf{e}}_i^m]\sum_{q=1}^{Q}\beta_q^{i,m}P_q^{i,m}(\mathbf{r})+[\mathbf{a}_k^n \cdot \hat{\mathbf{e}}_k^n]\sum_{q=1}^{Q}\beta_q^{k,n}P_q^{\mathrm{k},n}(\mathbf{r})=0, \quad \mathbf{r}\in \ell_c \ . \tag{41}$$

Enforcing the constraints in (41) at $N_p = p+1$ distinct points along ℓ_c allows us to write the matrix equation

$$\left[\left[C^{i,m}\right] \ \left[C^{k,n}\right]\right]\begin{bmatrix}\bar{\beta}^m \\ \bar{\beta}^n\end{bmatrix}=\bar{0} \tag{42}$$

where the superscripts i and k indicate the edge numbers on the m^{th} and n^{th} cells, respectively, and

$$\begin{aligned} C_{pq}^{k,n} &= [\mathbf{a}_k^n(\mathbf{r}_p)\cdot\hat{\mathbf{e}}_k^n(\mathbf{r}_p)]P_q^{k,n}(\mathbf{r}_p), \quad \mathbf{r}_p\in\ell_k^n \\ C_{pq}^{i,m} &= [\mathbf{a}_i^m(\mathbf{r}_p)\cdot\hat{\mathbf{e}}_i^m(\mathbf{r}_p)]P_q^{i,m}(\mathbf{r}_p), \quad \mathbf{r}_p\in\ell_i^m \end{aligned} \ . \tag{43}$$

The constraint in (42) is combined with the constraint that the normal components along the edges opposite the shared edge be zero to form the complete edge basis constraint matrix

$$\begin{bmatrix}[C^{i+2,m}] & [0] \\ [C^{i,m}] & [C^{k,n}] \\ [0] & [C^{k+2,n}]\end{bmatrix}\begin{bmatrix}\bar{\beta}^m \\ \bar{\beta}^n\end{bmatrix}=[C^{edge}]\bar{\beta}=\bar{0} \ , \tag{44}$$

where $[0]$ signifies an appropriately sized zero matrix block.

Once a constraint matrix $\left[C\right]$ is assembled, solutions to (37) and (44) are found using the SVD of $[C]$ as

$$[C]=[U][\Sigma][V]^H \ , \tag{45}$$

or, because $[U]$ and $[V]$ are unitary matrices,

$$[C][V] = [U][\Sigma]. \tag{46}$$

As will be discussed in the following section, a proper selection of functions $P_q(\mathbf{r})$ and sampling points $\mathbf{r}_p$ will make $[C]$ rank deficient, and $[\Sigma]$ will contain zero singular values. Let $[V_0]$ be the column vectors of $[V]$ corresponding to these singular values. The column vectors of $[V_0]$, therefore, are a basis for the null space of $[C]$, and each column vector $\bar{v}_{0,\mathrm{p}}$ of $[V_0]$ is a solution to (37) or (44). Finding these vectors is all that is required to construct the face bases, whose normal component must merely go to zero at the opposite edges of their associated cell.

The edge bases, on the other hand, represent currents flowing across the shared edge. Since (42) is also satisfied by the vectors $\bar{v}'^{m}_{p} = \begin{bmatrix} \bar{v}^{m}_{0,p} \\ \bar{0} \end{bmatrix}$ and $\bar{v}'^{n}_{q} = \begin{bmatrix} \bar{0} \\ \bar{v}^{n}_{0,q} \end{bmatrix}$ for the adjacent face bases on the m^{th} and n^{th} cells, respectively, these components are represented in the resulting edge basis function and are redundant with the corresponding face bases. These redundant edge bases are not representative of non-zero current flowing across the edge. In other words, currents that go to zero at the shared edge also satisfy continuity at the edge, but these currents are represented by the face bases and must be eliminated to leave only edge bases that represent currents continuous and non-zero at the shared edge. This can be accomplished by projecting the column vectors in $[V_0]$ for the edge onto those for the adjacent faces $[V_0^m]$ and subtracting the projection from the edge null space to get the projected matrix $[P]$. Here, $[P]$ is given by

$$[P] = [V_0] - [v'_m][v'_m]^T[V_0] - [v'_n][v'_n]^T[V_0] \ , \tag{47}$$

where the $[v'_m]$ matrices are made up of the vectors $\bar{v}'^{m}_{p}$. Finally, the SVD of $[P]$ is taken:

$$[P] = [U^P][\Sigma^P][V^P]^H \ . \tag{48}$$

The column vectors in $[U]$ corresponding to *non-zero* singular values in $[\Sigma]$ make up a basis for the projected null space generated by $[P]$, and are therefore used as the coefficient vectors for the edge bases.

2.5. Choice of Underlying Function Set

An advantage of the constrained basis approach is the freedom to choose the underlying function set $\{P_n(\mathbf{r})\}$, from which the basis functions are built, without any significant modification of program code. These functions must meet certain criteria and can significantly impact the efficiency of the numerical solution. In this thesis, we choose a mixed-order basis set of Legendre polynomials $P_n(x)$, so that a p^{th} order basis on the q^{th} cell has the form

$$\mathbf{B}_i^q(u^i, u^{i+1}) = \frac{\mathbf{a}_i}{\sqrt{g}} \sum_{m=0}^{p+1} \sum_{n=0}^{p} \beta_{mn}^q P_m(u^i) P_n(u^{i+1}) \tag{49}$$

where $\sqrt{g}$ is the surface Jacobian calculated at (u^i, u^{i+1}). These bases, of order (p+1) and p in the u^i and u^{i+1} directions, respectively, have the advantage mentioned above of an order-p complete representation of the charge, which helps avoid spurious resonances. Furthermore, the Legendre polynomials obey the orthogonality property

$$\left\langle P_m(x), P_n(x)\right\rangle = \int_{-1}^{1} P_m(x)P_n(x)dx = \frac{2}{2n+1}\delta_{mn} \ . \tag{50}$$

Following [1], the polynomials are scaled to obtain the scaled Legendre polynomials $\tilde{P}_n(x)$

$$\tilde{P}_n(x) = \sqrt{\frac{2n+1}{2}}P_n(x) \ , \tag{51}$$

which implies, according to (50),

$$\left\langle \tilde{P}_m(x), \tilde{P}_n(x)\right\rangle = \delta_{mn} \ . \tag{52}$$

This scaling is simple and its computational expense negligible, but it produces a marked improvement in matrix conditioning, as will be seen in the next chapter. This gives the final basis functions the form

$$\mathbf{B}_i^q(u^i, u^{i+1}) = \frac{\mathbf{a}_i}{\sqrt{g}} \sum_{m=0}^{p+1}\sum_{n=0}^{p} \beta_{mn}^q \tilde{P}_m(u^i)\tilde{P}_n(u^{i+1}) \, . \tag{53}$$

Due to the variation of $\mathbf{a}_i$ and $\sqrt{g}$, the orthogonality in (52) on ideal reference cells is not generally preserved when general curvilinear cells are used. Moreover, even on ideal reference cells, complete mutual orthogonality is not attained since edge bases are not orthogonalized with the overlapping face or edge bases defined on adjacent cells.

Using these scaled Legendre functions, the constraint matrices for face and edge bases have elements defined by

$$C_{ls}^{k,m} = \left[\frac{1}{\sqrt{g_s}} \mathbf{a}_i^m(\mathbf{r}_s) \cdot \hat{\mathbf{e}}_k^m(\mathbf{r}_s) \right] \tilde{P}_q(u^i)\tilde{P}_r(u^{i+1}), \quad \mathbf{r}_s \in (\ell_k^m), \quad k = i, i+2 \, , \tag{54}$$

where

$$l(q,r) = q(p+1) + r\,, \tag{55}$$

$\sqrt{g_s}$ is the surface Jacobian computed at $\mathbf{r}_s$, and u^i, u^{i+1} are the parameterized coordinates of the point $\mathbf{r}_s$ on the m^{th} cell. The particular $\mathbf{r}_s$ are chosen as the roots of the Legendre polynomials on the parameterized interval (0,1) along each constrained edge ℓ although other choices such as equally-spaced points should be suitable as well. The constraint matrix $[C]$ will have dimensions $2(p+1)\times(p+1)(p+2)$ for face bases and $3(p+1)\times 2(p+1)(p+2)$ for edge bases. Since $2(p+2) > 3$ for $p \geq 0$ and $(p+2) > 2$ for $p \geq 1$, the $[C^{edge}]$ and $[C^{face}]$ matrices will be rank deficient and have a null space for $p \geq 0$ and $p \geq 1$, respectively. The total number of bases N_{face} associated with each face and the number of bases N_{edge} associated with each edge (with redundancies removed) can be calculated as in [2]:

$$N_{face} = 2p(p+1) \tag{56}$$

$$N_{edge} = p+1\ . \tag{57}$$

In this chapter the derivation of a discretized MoM formulation from the field integral equations is summarized. The constrained basis approach is then introduced and used to generate divergence-conforming bases on quadrilateral cells for a MoM formulation. In the next chapter, numerical results showing accuracy and system conditioning demonstrate the effectiveness of the method.

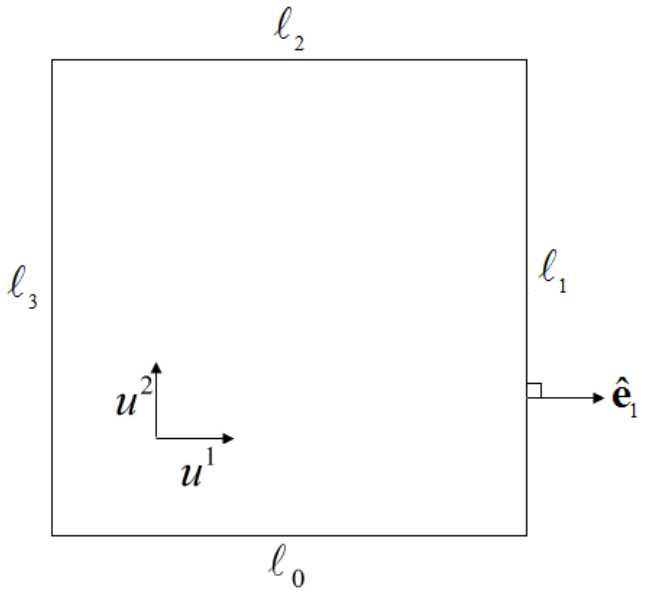

Figure 1: Parameterized coordinate and edge notation for quadrilateral cell

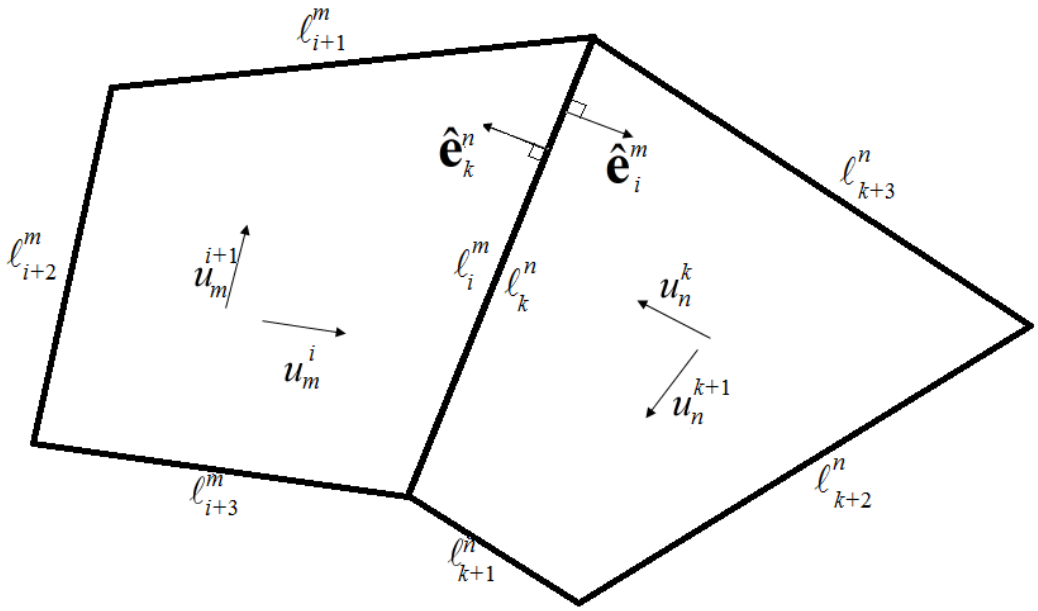

Figure 2: Parameterized coordinate and edge notation for adjacent quadrilateral cells

3. NUMERICAL RESULTS

In this chapter, the accuracy and efficiency of solutions to electromagnetic scattering problems using the proposed constrained bases in a MoM code are investigated. All simulations use a Galerkin-like testing procedure, and the underlying function set consists of the scaled Legendre polynomials, unless otherwise specified. Accuracy is judged by the relative root-mean-square (RMS) error in the far-field radiation pattern scattered by a sphere or a cube. For comparison with other basis sets, condition numbers for various basis orders are computed for parallel-plate and corner reflector geometries. Finally, frequency sweeps for a PEC sphere show the effect of the CFIE on the matrix condition number as well as the effect of the constrained bases on the conditioning of the electric, magnetic, and combined field integral equation systems across a frequency range.

3.1. Accuracy

The far-field scattering of a plane wave from a PEC sphere can be computed analytically [17], and therefore presents the most obvious and objective standard for accuracy comparison. Accuracy is gauged by the RMS error [18]

$$Error_{rms} = \sqrt{\frac{\Sigma_n \left| c(\theta_n) - a(\theta_n) \right|^2}{\Sigma_n \left| a(\theta_n) \right|^2}} \tag{58}$$

between the computed solution $c(\theta)$ and the reference solution $a(\theta)$, for θ from 0 to 180 degrees in 1-degree increments, at constant ϕ. First, a sphere of 1-meter radius was meshed with quadrilaterals and illuminated by a 50 MHz plane wave traveling in the $-\hat{z}$ direction. In Figure 3, the EFIE, MFIE, and CFIE cross-sections are compared to the analytic solution for the first 2 basis orders. Figure 4 and Figure 5 show the relative EFIE

solution error for constrained bases of order $p = 0,\ldots,5$ versus maximum mesh edge length. Also plotted is the relative error in the surface area of the discretized sphere. Here, p is the order to which the surface charge representation is polynomial complete and o is the mesh order where $o = 1$ indicates linear elements. In Figure 4, the mesh order is set to $o = p + 1$, and the resulting solution error is bounded below by the mesh discretization error. Accordingly, in Figure 5, the mesh order is set to $o = 1$ for $p = 0$ and $o = 2p$ for $p = 1,2,\ldots$. The resulting solution errors for basis orders $p > 1$ are now somewhat higher than the corresponding mesh errors, though solutions with even basis order show a significant increase in accuracy compared to the results in Figure 4.

3.1.1. Convergence

Figure 6, Figure 7, and Figure 8 show the EFIE, MFIE, and CFIE ($\alpha = 0.2$) error convergence, respectively, for basis orders $p = 0,\ldots,5$. A 10^{th} order sphere mesh is used to eliminate the effects of mesh error. The exponential convergence rates for all three formulations are shown in Table 1.

The cause of the MFIE divergence at higher orders has not yet been ascertained. A likely explanation is a loss of singularity cancellation due to numerical precision. The integral term in (2) can be rewritten as

$$\hat{\mathbf{n}} \times \nabla \times \iint_S \mathbf{J}(\mathbf{r}') G(\mathbf{r},\mathbf{r}')\, dS' = \iint_S \hat{\mathbf{n}} \times \nabla G(\mathbf{r},\mathbf{r}') \times \mathbf{J}(\mathbf{r}')\, dS' \ . \tag{59}$$

Since $\nabla G = \exp(-jkR)\left[\, jk/R - 1/R^2 \,\right]\hat{\mathbf{R}}$, there is a $1/R^2$ singularity when $\mathbf{r}'$ and $\mathbf{r}$ become close to each other with the overlap of source and field domains. A Duffy integration[19] is used which cancels a $1/R$ singularity. Also, $\hat{\mathbf{R}} \times \mathbf{J}(\mathbf{r}')$ becomes

parallel to $\hat{\mathbf{n}}$, and $\left|\hat{\mathbf{n}}\times\hat{\mathbf{R}}\times\mathbf{J}(\mathbf{r}')\right|$ approaches 0 as R. The Duffy integration and vector cross products should cancel the $1/R^2$ singularity, but suspected numerical precision issues prevent $\left|\hat{\mathbf{n}}\times\hat{\mathbf{R}}\times\mathbf{J}(\mathbf{r}')\right|$ from approaching 0 as R when R is less than about the square root of machine precision. This produces divergence when higher orders of numerical integration bring source and field points too close to one another.

The far-field scattering for a sphere of solid dielectric material with $\epsilon_r = 10.0$ was also simulated (using the Müller formulation [20]). Analytic and numerical scattering cross-sections are plotted in Figure 9, and the relative error convergence in Figure 10. The first four basis orders converge similarly to those for the PEC sphere, though as with the MFIE simulations for the PEC sphere, the higher basis orders show some divergence for finer meshes.

As there exists no known analytic solution for far-field scattering from a cube, the scattering cross-section for a PEC cube meshed with 15,000 cells using the interpolatory Glisson-Wilton-Peterson (GWP) functions [4] with $p = 1$ is taken as a reference. RMS error comparison between this reference and constrained basis results is plotted in Figure 11.

While the solutions for the sharp-edged cube converge more slowly than those for the sphere (approximately as $h^{1.4}$ where h is the maximum edge length), convergence is nevertheless consistent and well-behaved. The use of a numerical reference becomes apparent at higher orders, where the constrained basis solution becomes more accurate than the GWP reference as the mesh is refined.

3.1.2. Integration Order Variation

Figure 12 shows the relative error in the PEC-sphere scattering problem when different fixed-point numerical integration orders are used for the field integration. Raising the integration order does bring about a small improvement in accuracy especially at higher orders, though the solution begins to stagnate for finer meshes when $p = 5$.

3.2. Matrix Conditioning

MoM system matrices for several different types of geometry were analyzed in order to demonstrate the effect of the constrained bases on system matrix conditioning. In Figure 13 the condition number resulting from the use of the GWP bases is compared to that from the constrained bases both with and without optimal scaling of the underlying function set. This comparison illustrates not only the much slower growth of the matrix condition number when the constrained bases are used but also the reduction by nearly an order of magnitude with a simple scaling of the underlying function set.

For comparison with the bases presented by Jorgenson et al in [1], two parallel-plate simulations were run. In the first case, two 6λ square plates with 1λ separation were meshed and the system matrix constructed for basis orders $p = 0,\ldots,5$. The discretization was varied to match the number of degrees of freedom (DOF) for each basis order to that in [1], as may be seen in Table 2. The condition numbers for the constrained bases, the interpolatory bases of [4], and the hierarchical Legendre bases of [1] are plotted in Figure 14.

As shown, the matrix conditioning stays relatively constant for the first 6 function orders, on the order of 10^2. Not only is this an order of magnitude lower than the conditioning achieved by the basis set in [1], but it shows no consistent or significant growth as the basis order increases.

For two circular plates with diameter 10λ and 1λ separation, the condition number is somewhat larger but still stays well below that of the interpolatory case and approximately an order of magnitude below the results in [1] at higher orders, as shown in Figure 15. Table 3 shows average cell dimensions and number of DOF for each basis order for comparison with the equivalent problem in [1].

In order to compare with the maximally orthogonal bases in [5], simulations like those above were performed for a 6λ PEC corner reflector. The number of DOF for each basis order, for comparison with [5], is shown in Table 4, and as may be seen in Figure 16, the resulting condition numbers are very similar to those in [5]. In addition, the scattering cross-section for a plane wave incident from $\theta = \phi = 45^\circ$ is plotted in Figure 17.

In summary, the constrained basis functions compare well with and even improve significantly upon the matrix conditioning achieved by other highly-orthogonal Legendre-based bases.

3.3. Frequency Behavior

From [17], the first four TE and TM resonant frequencies for a PEC spherical cavity are 0.13093, 0.18465, 0.21438, and 0.23728 GHz. Simulation sweeps over this frequency range using both the constrained bases and the interpolatory bases of [4] were

run with EFIE, MFIE, and CFIE formulations. The system conditioning is shown in Figure 18 for both methods and all formulations, and one sees not only the successful elimination of the spurious resonances by the use of the CFIE, but also the consistency with which the constrained basis matrix conditioning stays approximately 3 orders of magnitude below that of the interpolatory cases across the entire frequency range for all formulations.

3.4. Timing

Taking the SVD of an $m \times n$ matrix is a comparatively expensive computation, and while this makes the solution of entire MoM system matrices by SVD impracticable, the constraint matrices here for basis order p have dimensions not greater than $3(p+1) \times 2(p+1)(p+2)$. For functions with $p = 0,1,...,5$, as Figure 19 illustrates, these bases are found to have a cost comparable to that of the interpolatory bases. This is in spite of the constraint matrix being formed and factored for every cell pair, a redundancy which could readily be removed by storing the basis function coefficients after the initial computation.

Table 1: Convergence rates h^{α} (α listed) for 10th order sphere

Formulation \ p	0	1	2	3	4	5
EFIE	3.0	4.0	5.8	5.0	7.1	7.1
MFIE	2.0	4.0	6.1	4.19*	7.9	***
CFIE	2.0	4.0	5.7	4.9**	7.1*	8.9*

*used first 2 points
**used last 3 points
***did not converge

Table 2: Quad cell size in wavelengths and number of DOF for each basis order in square parallel plates test

Basis order p	0	1	2	3	4	5
Quad Size $[\lambda]$	0.38	0.38	0.6	0.86	1.0	1.2
DOF	960	3968	3480	3024	3480	3480

Table 3: Quad cell size in wavelengths and number of DOF for each basis order in circular parallel plates test

Basis order *p*	0	1	2	3	4	5	6
Quad Size [λ]	0.36	0.36	0.65	0.92	0.94	1.61	1.61
DOF	2514	10148	7482	7656	8310	4980	6790

Table 4: Quad cell size in wavelengths and number of DOF for each basis order in corner reflector test

Basis order p	0	1	2	3	4	5	6	7
Quad Size[λ]	1/8	1/3	2/3	1	1.2	1.5	2.0	2.0
DOF	13680	7668	4293	3384	3675	3384	2583	3384

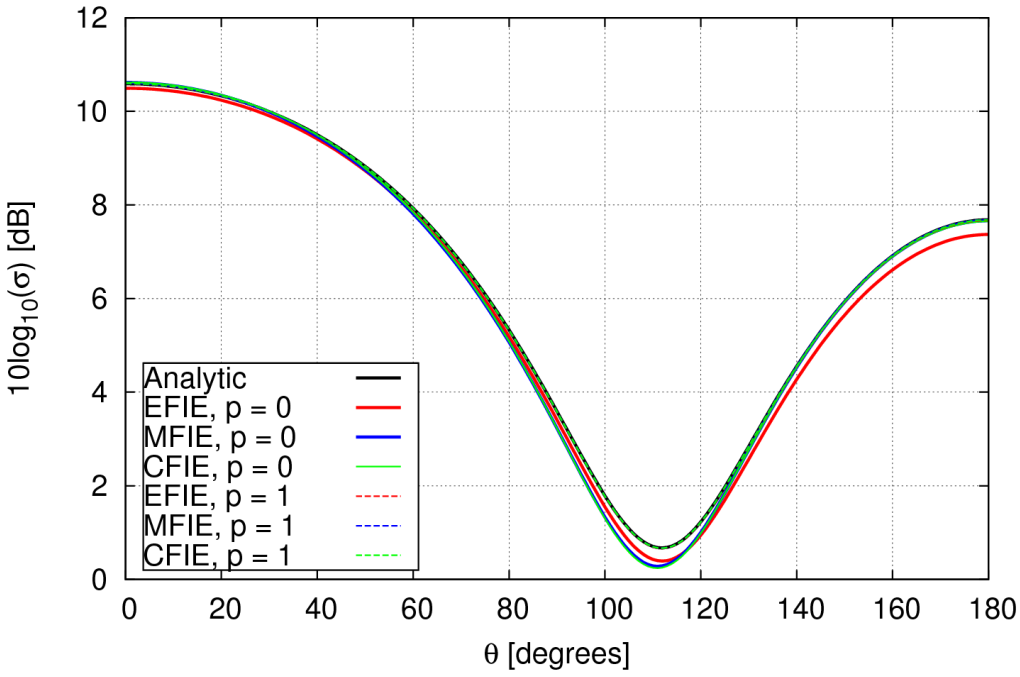

Figure 3: Scattering cross section for basis orders p = 0,1 with 1-m PEC sphere discretized with 24 quad cells at 50 MHz

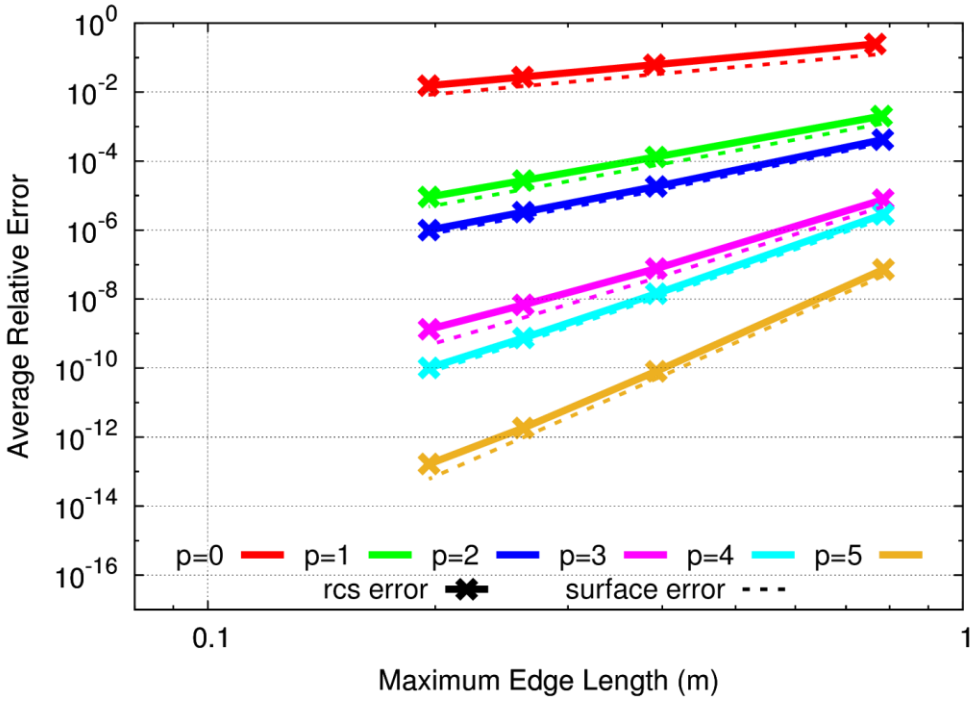

Figure 4: Average far-field relative error for 1-meter radius sphere at 50 MHz using EFIE. Constrained basis order is $p = 0,\ldots,5$, and mesh order is $o = p+1$. Integration tolerance is 10^{-8} .

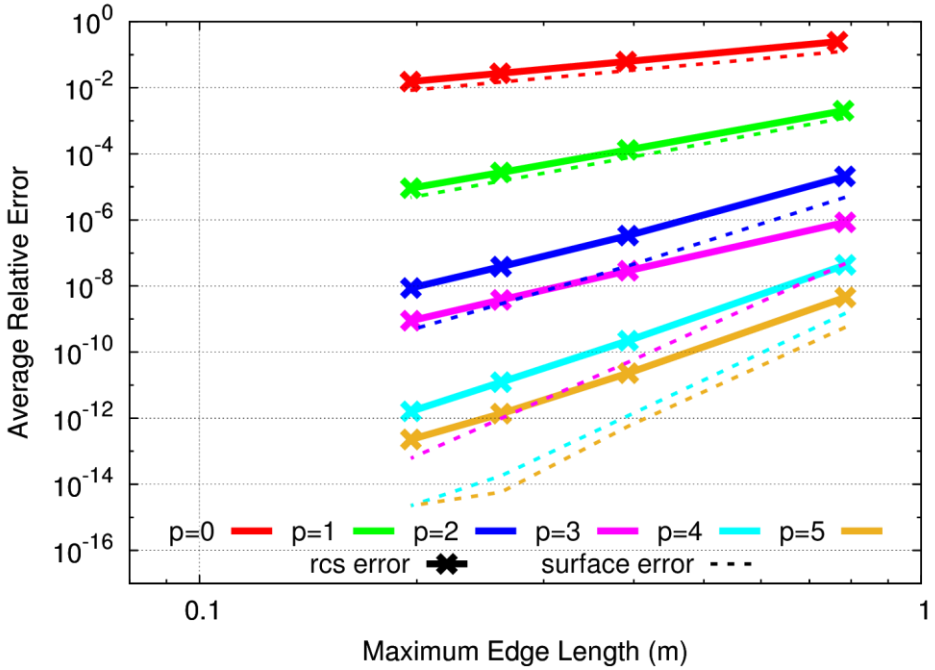

Figure 5: Average far-field relative error for 1-meter radius sphere at 50 MHz using EFIE. Constrained basis order is $p = 0,\ldots,5$, and mesh order is $o = 1$ for $p = 0$ and $o = 2p$ for $p = 1,2,\ldots$. Integration tolerance is 10^{-11}.

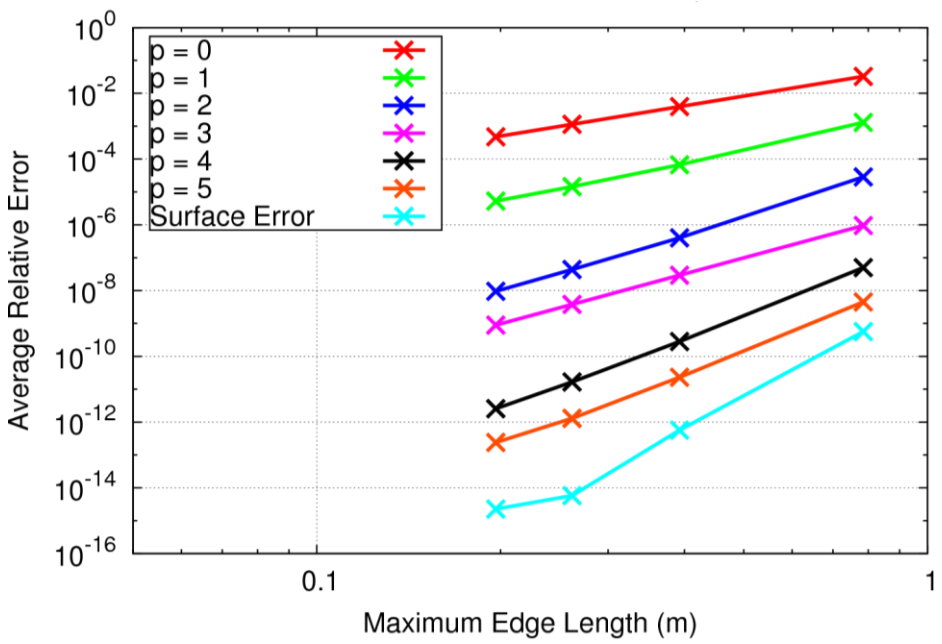

Figure 6: Average far-field relative error for 1-meter radius sphere at 50 MHz using EFIE. Constrained basis order is $p = 0,\ldots,5$, and mesh order is $o = 10$. Integration tolerance is 10^{-8}.

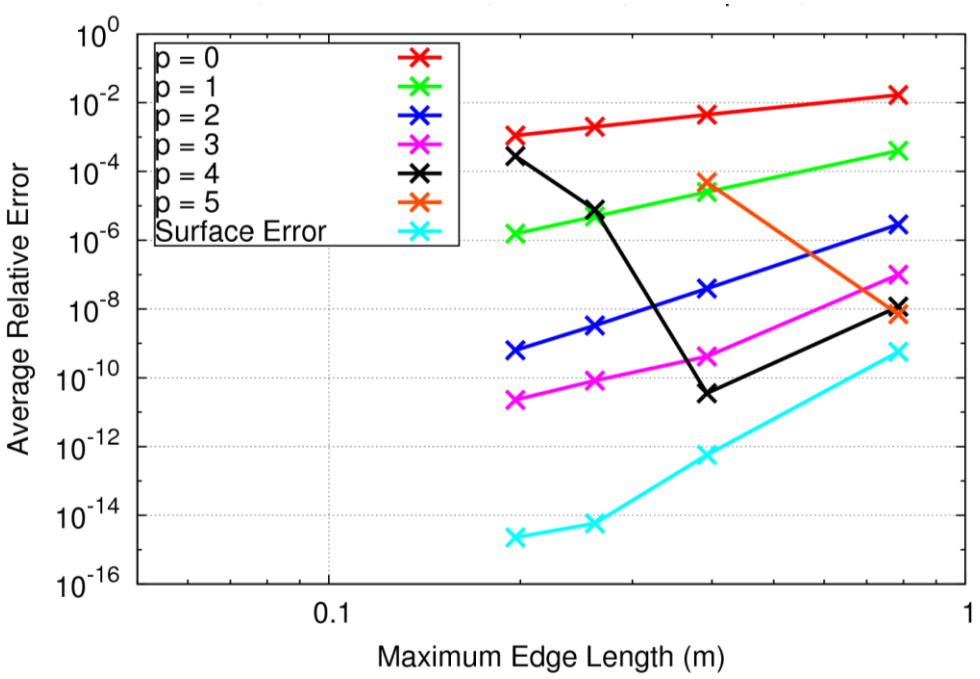

Figure 7: Average far-field relative error for 1-meter radius sphere at 50 MHz using MFIE. Constrained basis order is $p = 0,\ldots,5$, and mesh order is $o = 10$. Integration tolerance is 10^{-6}.

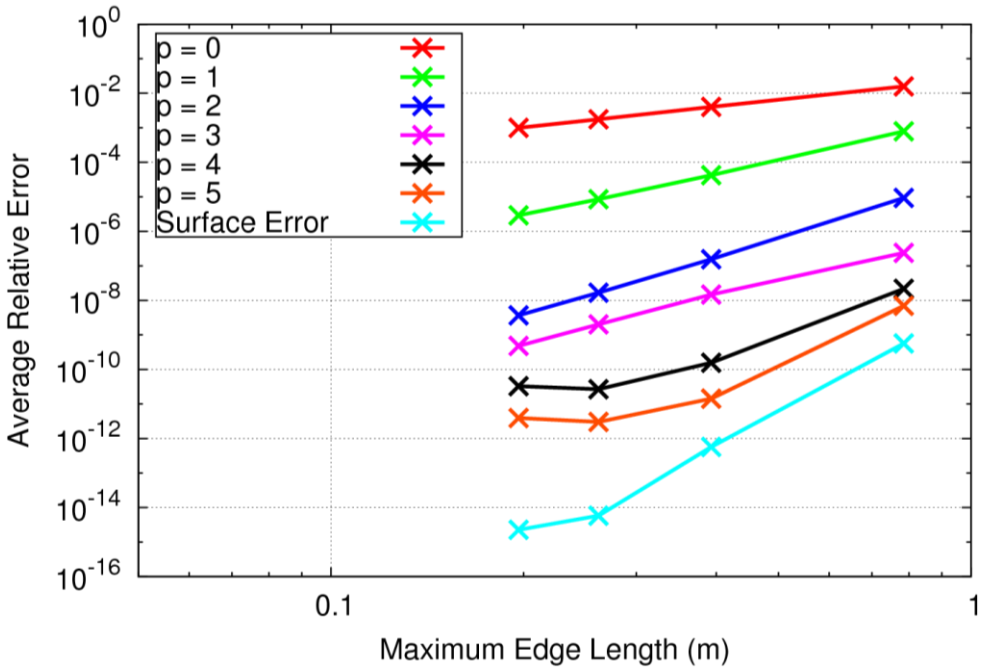

Figure 8: Average far-field relative error for 1-meter radius sphere at 50 MHz using CFIE. Constrained basis order is $p = 0,\ldots,5$, and mesh order is $o = 10$. Integration tolerance is 10^{-8}.

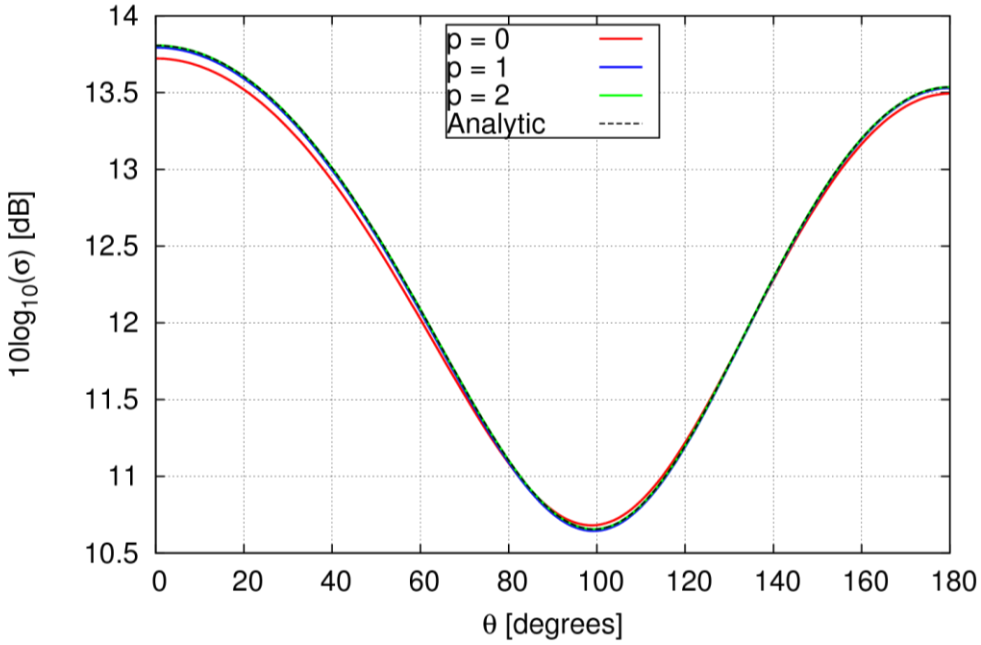

Figure 9: Far field radiation pattern for 1-meter dielectric sphere with ϵ_r=10 at 50 MHz. Integration tolerance is 10^{-8}.

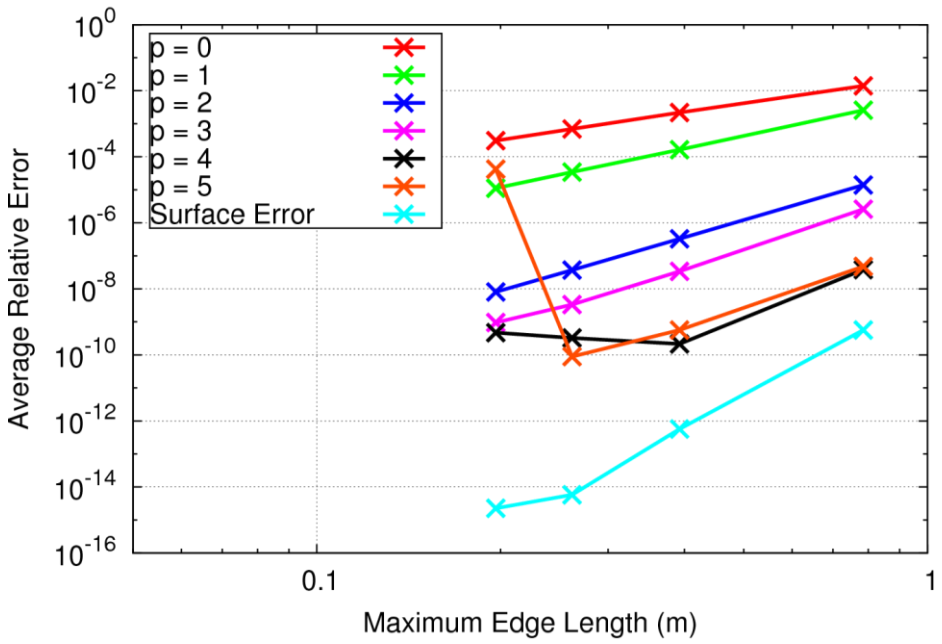

Figure 10: Accuracy convergence for dielectric sphere far-field scattering at 50 MHz. Integration tolerance is 10^{-8}

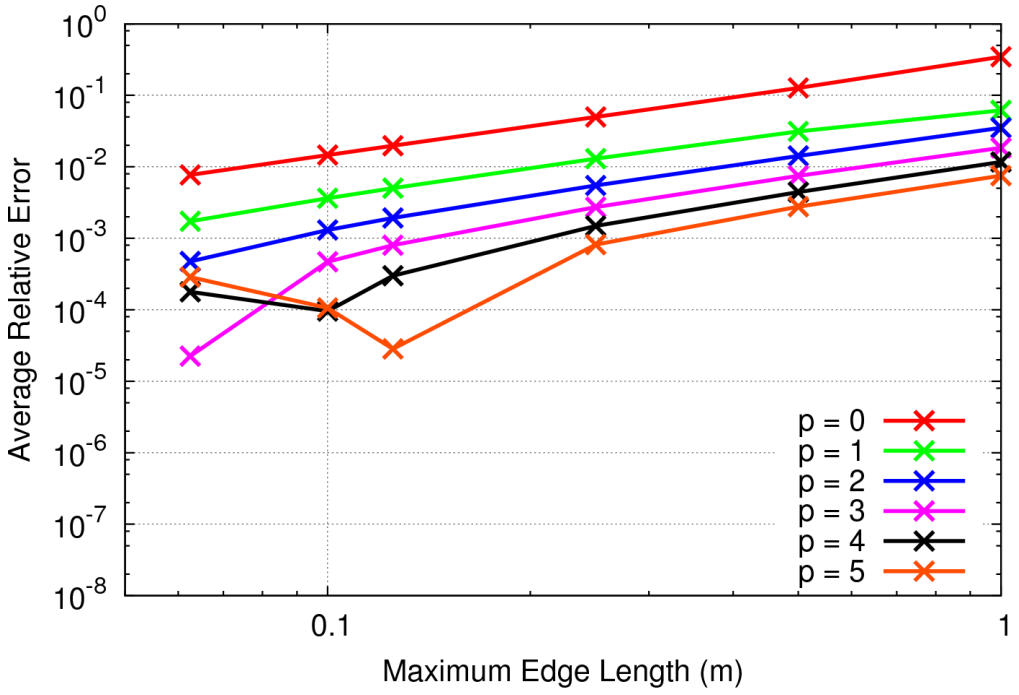

Figure 11: EFIE relative error for 1-meter PEC cube at 50MHz. Integration tolerance is 10^{-8}

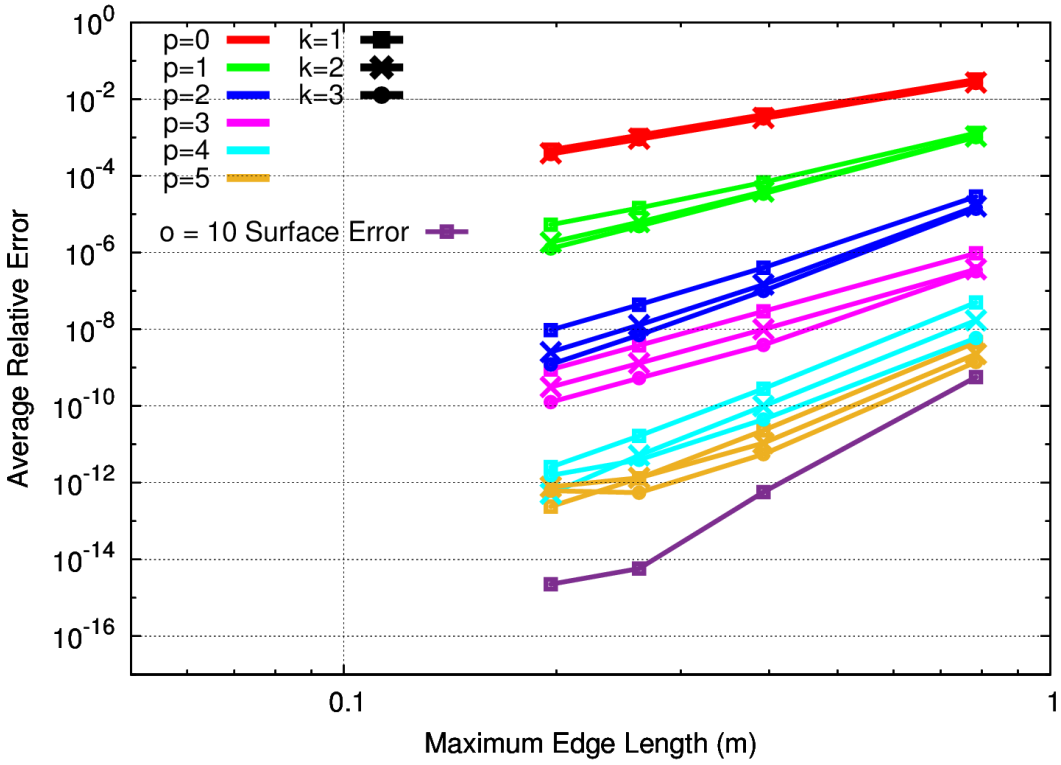

Figure 12: EFIE convergence rates for 1-meter PEC sphere far-field scattering at 50 MHz, with integration order (p+k) for k = 1,2,3 Integration tolerance is 10^{-8}.

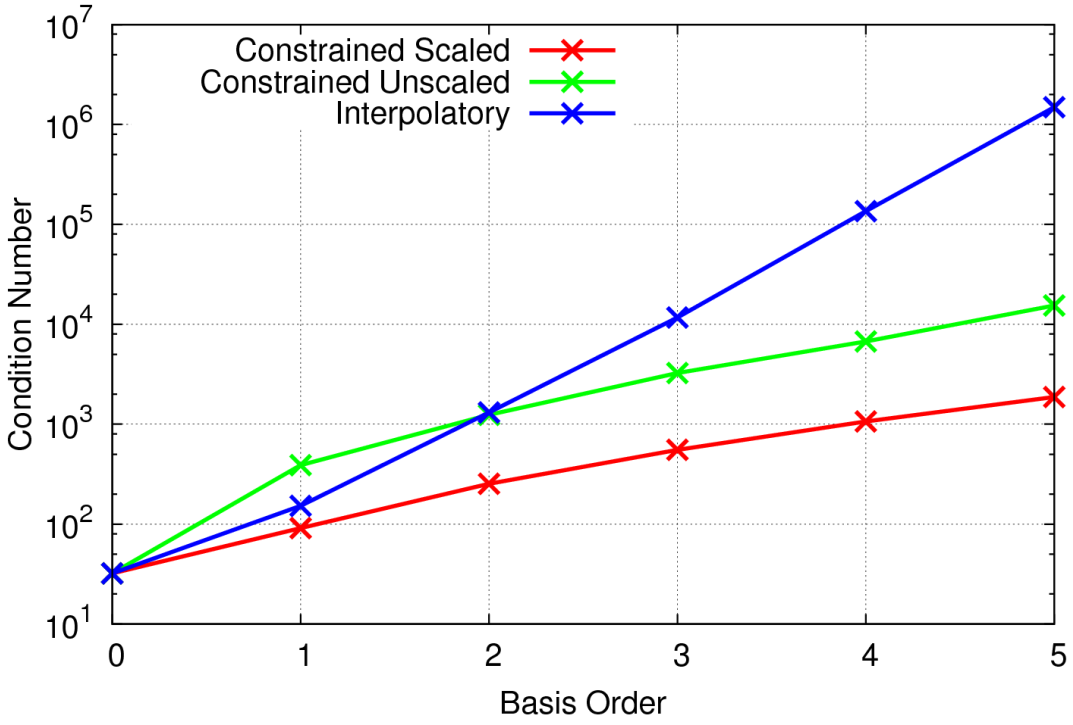

Figure 13: Comparison of EFIE matrix condition numbers for different bases for a 1-meter PEC sphere discretized with 384 quadrilateral cells at 300MHz. Integration tolerance is 10^{-8}.

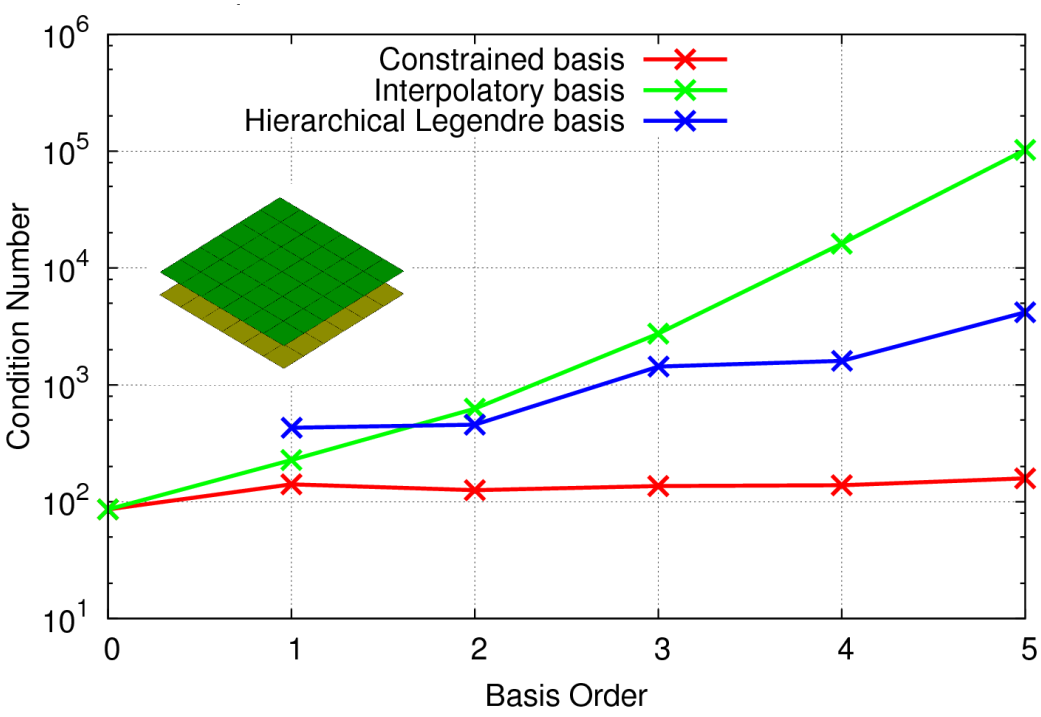

Figure 14: EFIE condition numbers for constrained, interpolatory, and Hierarchical Legendre basis systems are compared for 6λ×6λ plates with 1λ separation at 300MHz. Integration tolerance is 10^{-8}.

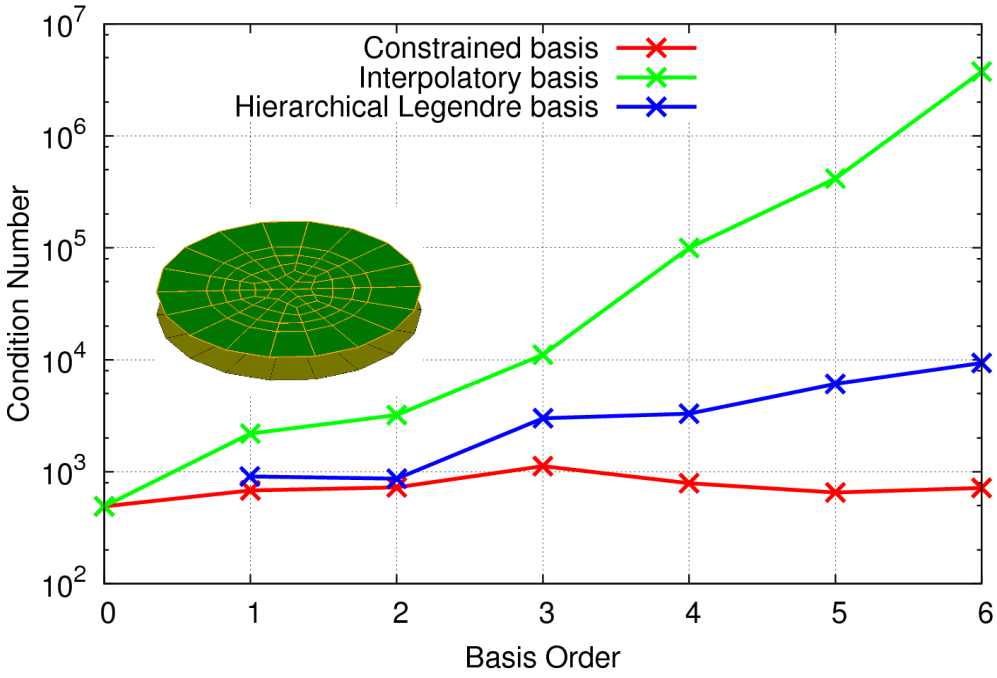

Figure 15: EFIE condition numbers for constrained, interpolatory, and hierarchical Legendre basis systems are compared for 10λ diameter plates with 1λ separation at 300MHz. Integration tolerance is 10^{-8}.

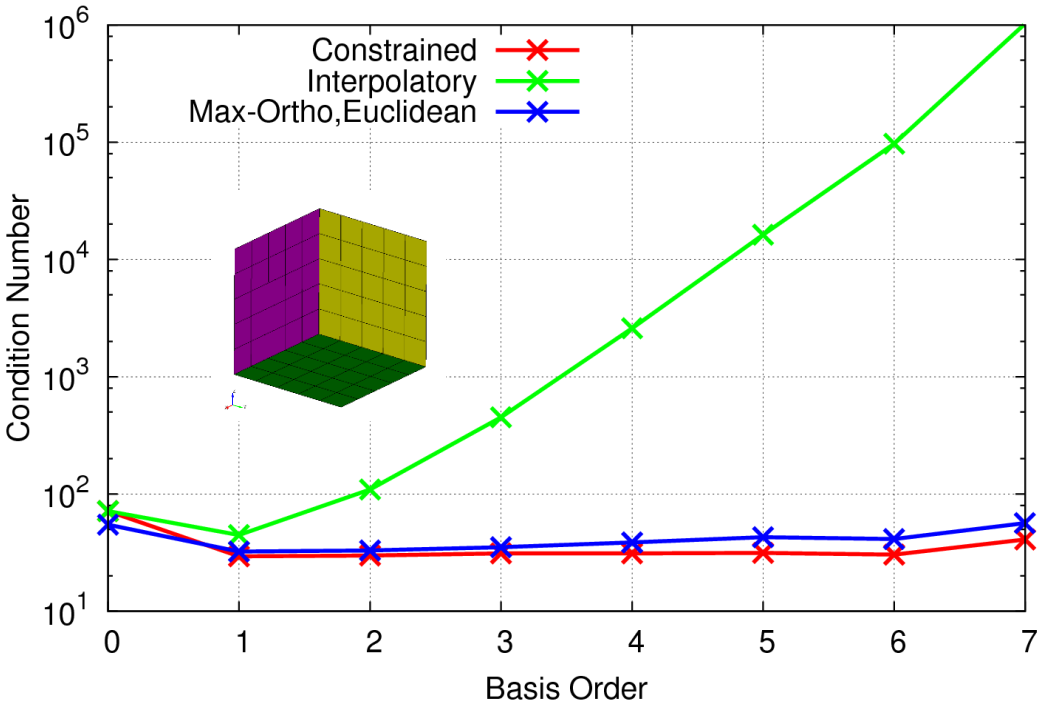

Figure 16: EFIE condition numbers for constrained, interpolatory, and max-ortho basis systems for 6λ corner reflector at 300MHz. Integration tolerance is 10^{-8}.

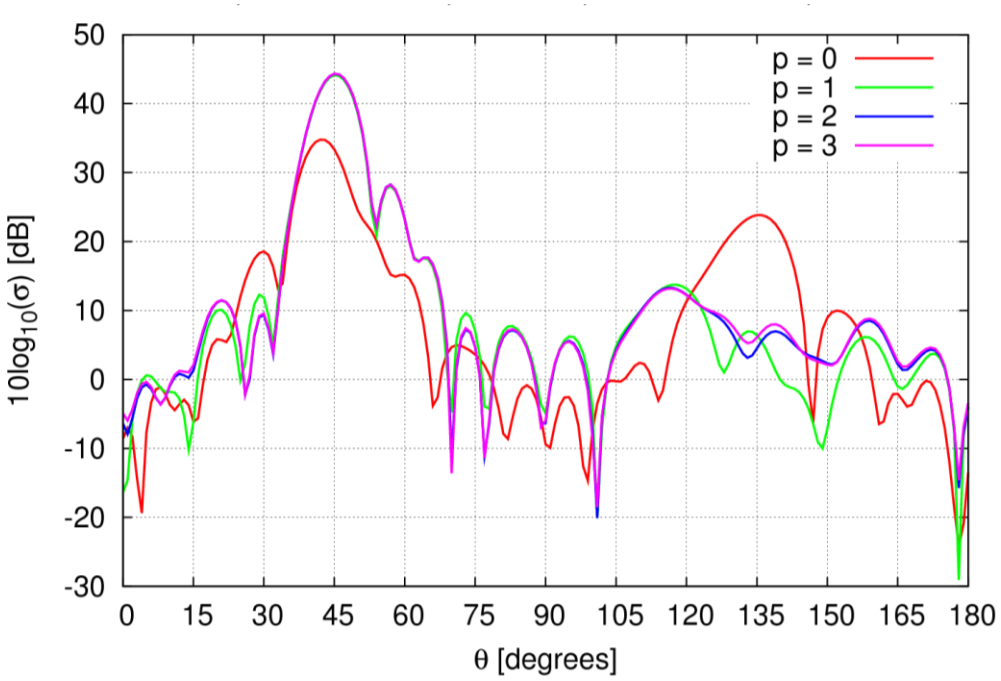

Figure 17: Far-field scattering from 6λ PEC corner reflector at φ = 45°. Integration tolerance is 10^{-8}.

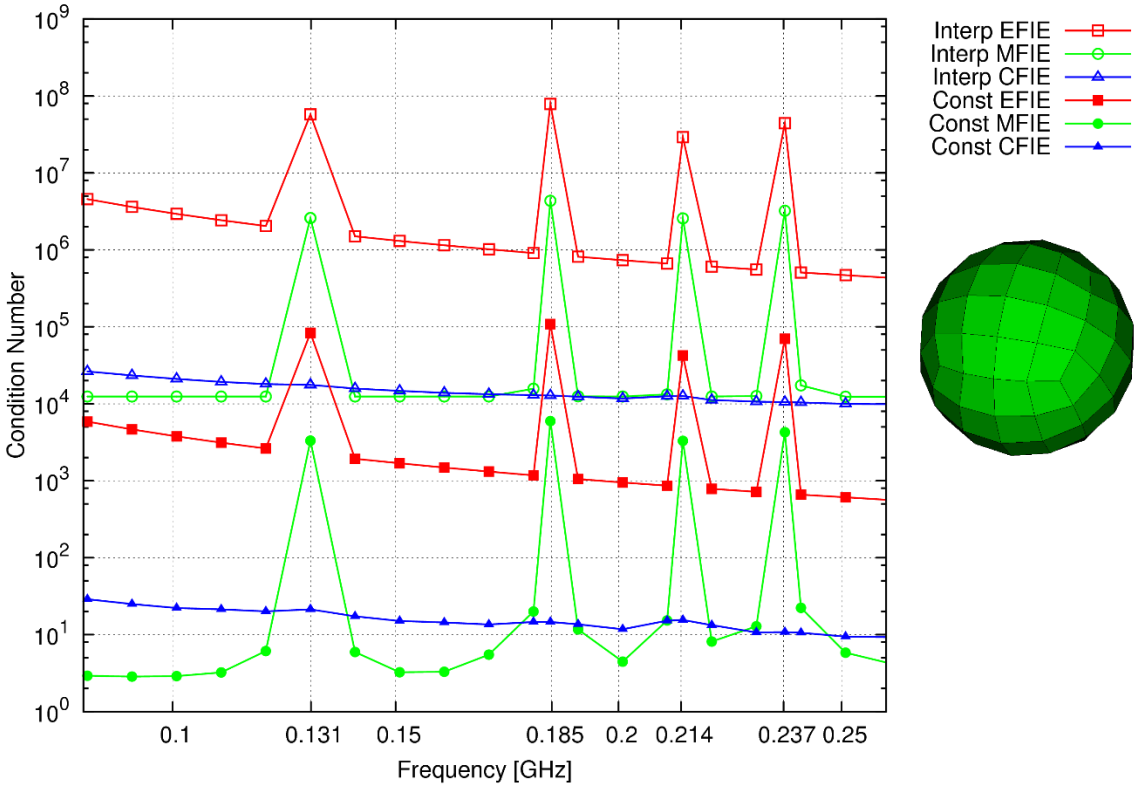

Figure 18: EFIE, MFIE, and CFIE condition numbers over first 4 resonant frequencies for sphere of radius 1-meter, plotted for both constrained and interpolatory bases. Integration tolerance is 10^{-8} for EFIE and CFIE formulations, 10^{-6} for MFIE.

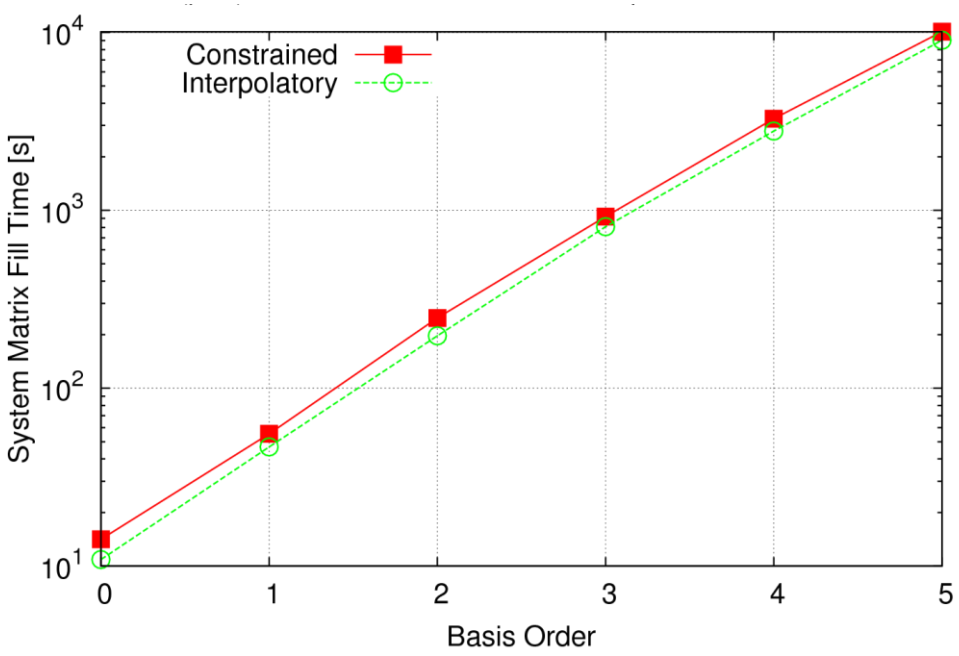

Figure 19: EFIE matrix fill time for 384-quad, 1-meter radius sphere at 50MHz using constrained and interpolatory bases. Mesh order is $o = p + 1$ .Integration tolerance is 10^{-8}.

4. CONCLUSION

In this thesis, a method for generating basis functions suitable for MoM discretizations of integral equations is presented, implemented, and validated. Constraints suitable for the construction of high-order divergence-conforming [18] bases on quadrilateral cells are discussed. The singular value decomposition of constraint matrices is used to produce bases that exhibit good accuracy and convergence characteristics, on par with interpolatory bases of the same order. This method of basis function generation is not limited to divergence-conforming bases but can in theory be used to impose other constraints such as curl-conformity with relatively minor program alterations. Moreover, the function set from which the bases are generated can be modified with similar ease.

A significant advantage of the constrained basis approach is the improved system conditioning achieved when a proper function set is chosen. In this thesis, the use of Legendre polynomials as the underlying function set gave good conditioning that increased slowly with basis order as compared to the interpolatory bases of [4]. Proper scaling of the Legendre polynomials, however, brought about even better conditioning, resulting in system matrices with conditioning comparable to or better than those reported [1, 5] for other highly orthogonal bases.

One of the most prominent features of the constrained bases is their versatility. Accordingly, many opportunities remain to extend their use into various areas of computational electromagnetics. Their application to triangular meshing has yet to be addressed, as well as to volume integral equations to reduce the number of required DOF and improve matrix conditioning. The application of the technique to locally-corrected Nyström discretizations [2, 8] based on augmented formulations [21, 22] is especially

appealing as it eliminates boundary charges [2]. Besides its use in integral equation methods, the constrained basis approach could readily be used in other methods, for instance, to generate the curl-conforming bases in finite element formulations.

REFERENCES

[1] E. Jorgensen, J. L. Volakis, P. Meincke, and O. Breinbjerg, "Higher order hierarchical Legendre basis functions for electromagnetic modeling," *IEEE Transactions on Antennas and Propagation,* vol. 52, pp. 2985-2995, Nov 2004.

[2] N. Hendijani, J. Cheng, R. J. Adams, and J. C. Young, "Constrained Locally Corrected Nystrom Method," *IEEE Transactions on Antennas and Propagation,* vol. 63, pp. 3111-3121, Jul 2015.

[3] B. M. Kolundzija and B. D. Popovic, "Entire-Domain Galerkin Method for Analysis of Metallic Antennas and Scatterers," *IEE Proceedings-H Microwaves Antennas and Propagation,* vol. 140, pp. 1-10, Feb 1993.

[4] R. D. Graglia, D. R. Wilton, and A. F. Peterson, "Higher order interpolatory vector bases for computational electromagnetics," *IEEE Transactions on Antennas and Propagation,* vol. 45, pp. 329-342, Mar 1997.

[5] M. M. Kostic and B. M. Kolundzija, "Maximally Orthogonalized Higher Order Bases Over Generalized Wires, Quadrilaterals, and Hexahedra," *IEEE Transactions on Antennas and Propagation,* vol. 61, pp. 3135-3148, Jun 2013.

[6] J. P. Webb, "Hierarchal Vector Basis Functions of Arbitrary Order for Triangular and Tetrahedral Finite Elements," *IEEE Transactions on Antennas and Propagation,* vol. 47, pp. 1244-1253, Aug 1999.

[7] D. S. Sumic and B. M. Kolundzija, "Efficient iterative solution of surface integral equations based on maximally orthogonalized higher order basis functions," in *Antennas and Propagation Society International Symposium, 2005 IEEE*, 2005, pp. 288-291 vol. 4A.

[8] N. Hendijani, "The Constrained Locally Corrected Nyström Method," Doctor of Philosophy (PhD) Doctoral Dissertation, Electrical and Computer Engineering, University of Kentucky, 2015.

[9] J. Cheng, "Formulation and solution of electromagnetic integral equations using constraint-based Helmholtz decompositions," Doctor of Philosophy (PhD) Doctoral Dissertation, Electrical and Computer Engineering, University of Kentucky, Lexington, Ky., 2012.

[10] J. Cheng and R. J. Adams, "Electric Field-Based Surface Integral Constraints for Helmholtz Decompositions of the Current on a Conductor," *IEEE Transactions on Antennas and Propagation,* vol. 61, pp. 4632-4640, Sep 2013.

[11] S. M. Rao, D. Wilton, and A. W. Glisson, "Electromagnetic Scattering by Surfaces of Arbitrary Shape," *Antennas and Propagation, IEEE Transactions on,* vol. 30, pp. 409-418, 1982.

[12] C. A. Balanis, *Advanced engineering electromagnetics*. New York: Wiley, 1989.

[13] A. F. Peterson, S. L. Ray, R. Mittra, and IEEE Antennas and Propagation Society., *Computational methods for electromagnetics*. New York, Oxford: IEEE Press ; Oxford University Press, 1998.

[14] C.-T. Chen, *Linear system theory and design,* 3rd ed. New York: Oxford University Press, 1999.

[15] J. A. Stratton, *Electromagnetic Theory*. New York: McGraw-Hill, 1941.

[16] S. D. Gedney, A. Zhu, and C. C. Lu, "Study of Mixed-Order Basis Functions for the Locally-Corrected Nyström Method," *IEEE Transactions on Antennas and Propagation,* vol. 52, pp. 2996-3004, November 2004.
[17] R. F. Harrington, *Time-Harmonic Electromagnetic Fields*, 2nd ed. New York: Wiley-IEEE Press, 2001.
[18] A. F. Peterson, *Mapped Vector Basis Functions for Electromagnetic Integral Equations*, 1st ed. San Rafael, Calif.: Morgan & Claypool Publishers, 2005.
[19] J. L. Volakis and K. Sertel, *Integral equation methods for electromagnetics*. Raleigh, NC: SciTech Pub., 2011.
[20] P. Yla-Oijala and M. Taskinen, "Well-conditioned Muller formulation for electromagnetic scattering by dielectric objects," *Ieee Transactions on Antennas and Propagation,* vol. 53, pp. 3316-3323, Oct 2005.
[21] Z. G. Qian and W. C. Chew, "An augmented electric field integral equation for highspeed interconnect analysis," *Microwave and Optical Technology Letters,* vol. 50, pp. 2658-2662, Oct 2008.
[22] J. C. Young, Y. Xu, R. J. Adams, and S. D. Gedney, "High-Order Nyström Implementation of an Agumented Electric Field Integral Equation," *IEEE Antennas and Wireless Propagation Letters,* vol. 11, pp. 846-849, 2012.

VITA

Robert Pfeiffer received a B.A. in Liberal Arts from Thomas Aquinas College, Santa Paula, CA, in May of 2012. He studied Electrical Engineering at the Milwaukee School of Engineering in Milwaukee, WI, from September 2012 to May 2014. He worked as an engineering intern for Johnson Controls Inc. in Milwaukee, WI, from June 2013 to August 2014. He has been working as a graduate research assistant at the University of Kentucky, Lexington, KY, since August 2014.